Title

Case History: Using time-lapse vertical seismic profiling data to constrain velocity–saturation relations: the Frio brine pilot CO2 injection

Journal

Geophysical Prospecting, 64(4)

ISSN

0016-8025

Authors

Hosni, Mohammed Al
Caspari, Eva
Pevzner, Roman
et al.

Publication Date

2016-07-01

DOI

10.1111/1365-2478.12386

Peer reviewed

Case History: Using time-lapse vertical seismic profiling data to constrain velocity–saturation relations: the Frio brine pilot CO_2 injection

Mohammed Al Hosni[1,2]*, Eva Caspari[5], Roman Pevzner[1,2], Thomas M. Daley[4] and Boris Gurevich[1,2,3]

[1]Department of Exploration Geophysics, Curtin University, GPO Box U1987, Perth, WA 6845, Australia, [2]Cooperative Research Centre for Greenhouse Gas Technologies (CO2CRC), Barton, ACT 2600, Australia, [3]CSIRO Energy, 26 Dick Perry Avenue, ARRC, Kensington, WA 6151, Australia, [4]Lawrence Berkeley National Laboratory, 1 Cyclotron Road, Berkeley, CA 94720 USA, and [5]Applied and Environmental Geophysics Group, University of Lausanne, 1015 Lausanne, Switzerland

∗E-mail: m.alhosni@postgrad.curtin.edu.au

ABSTRACT

CO_2 sequestration projects benefit from quantitative assessment of saturation distribution and plume extent for field development and leakage prevention. In this work, we carry out quantitative analysis of time-lapse seismic by using rock physics and seismic modelling tools. We investigate the suitability of Gassmann's equation for a CO_2 sequestration project with 1600 tons of CO_2 injected into high-porosity, brine-saturated sandstone. We analyze the observed time delays and amplitude changes in a time-lapse vertical seismic profile dataset. Both reflected and transmitted waves are analyzed qualitatively and quantitatively. To interpret the changes obtained from the vertical seismic profile, we perform a 2.5D elastic, finite-difference modelling study. The results show a P-wave velocity reduction of 750 m/s in the proximity of the injection well evident by the first arrivals (travel-time delays and amplitude change) and reflected wave amplitude changes. These results do not match with our rock physics model using Gassmann's equation predictions even when taking uncertainty in CO_2 saturation and grain properties into account. We find that time-lapse vertical seismic profile data integrated with other information (e.g., core and well log) can be used to constrain the velocity–saturation relation and verify the applicability of theoretical models such as Gassmann's equation with considerable certainty. The study shows that possible nonelastic factors are in play after CO_2 injection (e.g., CO_2–brine–rock interaction and pressure effect) as Gassmann's equation underestimated the velocity reduction in comparison with field data for all three sets of time-lapse vertical seismic profile attributes. Our work shows the importance of data integration to validate the applicability of theoretical models such as Gassmann's equation for quantitative analysis of time-lapse seismic data.

Key words: VSP, Rock physics, Time lapse, Monitoring.

INTRODUCTION

Sequestration of CO_2 into subsurface brine formations requires a monitoring and verification strategy that accounts for both the plume extent and saturation distribution in the subsurface. Time-lapse seismic has been identified as an effective tool for such requirements. In the last decade, time-lapse seismic was successfully used to detect CO_2 plumes using both surface seismic and vertical seismic profile (VSP) (e.g., Arts *et al*. 2004; Daley *et al*. 2008; Lüth *et al*. 2011). However, quantitative interpretation of velocity and amplitude changes is still a challenge (Lumley *et al*. 2008).

A common practice to quantitatively relate observed time-lapse seismic changes to reservoir properties is using a rock physics model that predicts the changes in the elastic properties corresponding to the changes in the reservoir properties (Johansen *et al*. 2013). A conventional way is to use Gassmann's poroelasticity theory (Gassmann 1951). Gassmann's theory assumes that the medium is homogeneous on both microscopic and macroscopic scales and also isotropic on the microscale. As noted by Brown and Korringa (1975), “Sedimentary materials, to which his theory is most often applied, do not even approximately satisfy the conditions of microhomogeneity and microisotropy”. In particular, in the context of time-lapse VSP, both direct and reflected waves sample large volumes of subsurface rocks, which might not satisfy this assumption. Therefore, in order to use Gassmann's theory at the seismic scale, it is essential to test its applicability at this scale using field data. This problem arises in many time-lapse monitoring projects such as enhanced oil recovery, production monitoring (Lumley 2001; Yang *et al*. 2014), and, more recently, CO_2 sequestration monitoring (e.g., Arts *et al*. 2004; Daley *et al*. 2008; Ivanova *et al*. 2012). Geophysical data acquired during CO_2 sequestration in saline aquifers such as Ketzin, Nagaoka, Otway, and Frio (Michael *et al*. 2010) provide high-resolution *in situ* data for calibration with theoretical rock physics. Thus, they present an attractive opportunity to investigate the applicability of theoretical models at the seismic scale.

The ability to perform such calibration relies on the resolution of the geophysical method used. Surface seismic has been successfully used to characterize large CO_2 volume like the Sleipner field (Arts *et al*. 2004; Chadwick *et al*. 2010). However, characterization of CO_2 accumulations in small-scale injection projects such as the Ketzin pilot is still challenging (Ivandic *et al*. 2012). For small-scale injection projects, VSP can minimize typical time-lapse monitoring challenges by providing better vertical and lateral resolution associated with high-frequency content and high signal-to-noise ratio (O'Brien, Kilbride, and Lim 2004). In the Frio project, comprehensive field measurements were acquired, including core, well logs, crosswell seismic, and VSP data (Sakurai *et al*. 2006; Daley *et al*. 2008; Doughty, Freifeld, and Trautz 2008). High-resolution VSP was conducted using the injection well for downhole receivers to acquire a multi-azimuth coverage of the CO_2 plume evolution (Daley *et al*. 2008). This allows the monitoring of the CO_2 plume using reflection amplitudes with high resolution

as the Fresnel zone is getting smaller with the decrease in the reflector–receiver distance (Hardage 1985). Moreover, travel-time changes and amplitudes of first arrivals going through the CO_2 plume provide another constraint on the reservoir seismic response to injected CO_2 (Zhou *et al*. 2010). Such information can be used to constrain the velocity–saturation relation (VSR) and highlight the uncertainty.

Daley *et al*. (2008) computed CO_2 saturation for the Frio "C" reservoir from VSP and crosswell data. This was done using a high-porosity sand model calibrated with the Utsira Sand of the Sleipner CO_2 North Sea data (Carcione *et al*. 2006) as not all the components required for the rock physics model were available (Daley *et al*. 2008; Doughty *et al*. 2008).

The goal of this paper is to investigate the use of time-lapse VSP data to constrain the drained frame properties for the rock physics model and the VSR of the Frio "C" reservoir based on the well log data of the Frio formation. To this end, we use direct and reflected waves to quantify the CO_2 effect on the formation. First, we analyze transmitted first-arrival travel times and amplitudes as they provide high signal-to-noise information for the CO_2 plume evaluation, followed by the analysis of reflection amplitudes. Second, we implement a forward modelling exercise using 2.5D elastic, finite-difference modelling (Kostyukevych *et al*. 2008) to predict the time-lapse VSP response and compare with the real data response. Third, we perform a quality check of the input parameters for the rock physics model, assessing the uncertainties and their effect on the drained frame properties' estimation. We employ the Gassmann fluid substitution workflow outlined in Smith, Sondergeld, and Rai (2003) to invert for the drained frame properties using well logs and subsequent fluid replacement. We conclude this paper with a discussion of the results highlighting the discrepancies observed between modelling and field data with their possible causes.

BOREHOLE SEISMIC MONITORING AT FRIO CO_2 INJECTION SITE

The Frio-I brine pilot study was an experimental small-scale CO_2 injection project conducted east of Houston, TX, USA (Hovorka 2009). The injection unit Frio "C" is a high-porosity and high-permeability sandstone that is part of the Oligocene Frio formation. Lithologically, Frio "C" is characterized as a subarkosic, moderately sorted sandstone with minor amounts of calcite (Kharaka *et al*. 2009). The formation is dipping about 16° to the south. The regional shales and siltstone Anahuac formation above the Frio formation act as a cap rock (Hovorka *et al*. 2006).

The injection of CO_2 took place in a purpose-drilled well about 30 m down-dip from an existing well that was used for observation of CO_2 breakthrough. A total of 1600 tons of CO_2 was injected at a depth of about 1540 m over a period of ten days using a 5.5-m perforated zone at the top section of the Frio "C" sandstone (Daley *et al*. 2008). A suite of conventional logs was obtained before injection, including sonic, density, gamma ray, and resistivity logs (Sakurai *et al*. 2006). A detailed geological and geochemical

characterization of the formation can be found in Hovorka *et al*. (2006) and Doughty *et al*. (2008).

A time-lapse VSP survey was acquired with the objective of mapping the CO_2 distribution around the vicinity of the injection well (Daley *et al*. 2008). The VSP geometry is shown in Fig. 1. Distribution of shot points was based on the dip of the formation as CO_2 was expected to migrate predominantly up-dip towards the north by gravity (Daley *et al*. 2008).

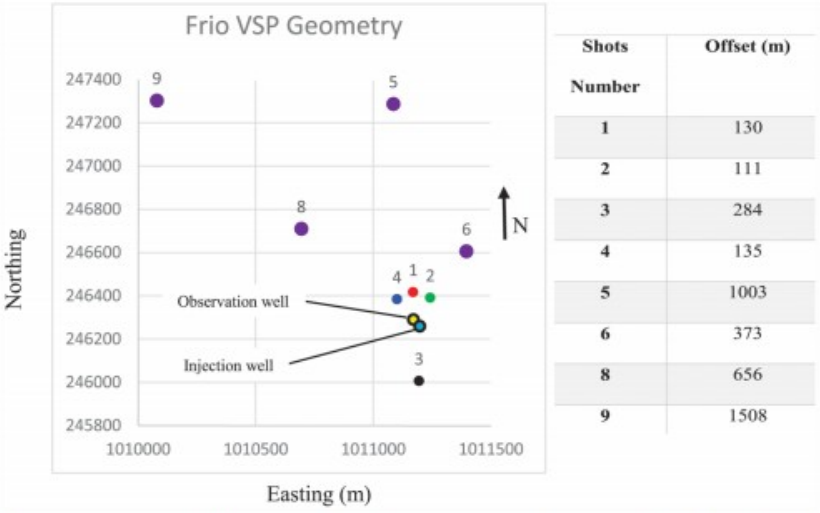

Shots Number	Offset (m)
1	130
2	111
3	284
4	135
5	1003
6	373
8	656
9	1508

Figure 1 Map view of Frio VSP geometry and table of shot offsets. Shots are numbered, and wells are indicated. Shots 1–4 are near the injection well with less than 300-m offset. Modified from Daley *et al.* (2008).

Eight shot points were acquired for various azimuths with an offset range from 110 m to 1500 m, approximately. As sources, dynamite charges weighing 1.6 kg each buried at a depth of 18.3 m below the surface were used (Daley *et al*. 2008). The receiver coverage in the injection well extended from the surface to a total well depth of 1686 m for shots 1 and 3 and from 1072 m to 1686 m for the other shots. The baseline survey was conducted before CO_2 injection, whereas the monitor survey was acquired about six weeks after the end of CO_2 injection. Similar source and receiver geometries were used for both surveys (Doughty *et al*. 2008).

VERTICAL SEISMIC PROFILE DATA PREPARATION AND PROCESSING

The aim of time-lapse VSP data processing is to extract the maximum amount of information related to time-lapse changes using both the upgoing and downgoing wavefields. The preparation of the time-lapse VSP data for first-arrival analysis does not involve amplitude or phase changing operators such as median filtering and deconvolution. However, for the P-wave upgoing wavefield analysis (i.e., reflection analysis), the processing sequence requires filtering to separate or remove unwanted seismic events such as downgoing wavefield, shear waves, multiples, and noise.

To prepare the raw data for subsequent processing, preliminarily processing is performed, which includes the removal of noisy traces and the application of field static shifts (see Fig. 2). These processes do not involve amplitude or phase changing operators. Figure 3 shows the first arrivals of the time-lapse VSP data after preprocessing. The first-arrival times of the monitor survey are expected to show a time delay (indicated in Fig. 3) due to changes in the velocities of the medium as CO_2 replaces brine.

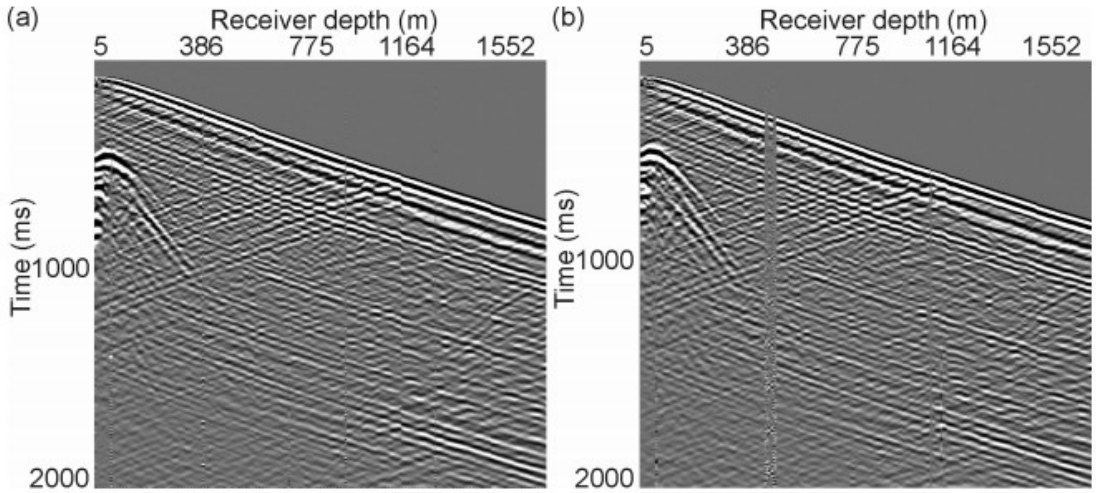

Figure 2 Raw shot record for Frio VSP after preprocessing. Shot 1: (a) pre-injection and (b) post-injection.

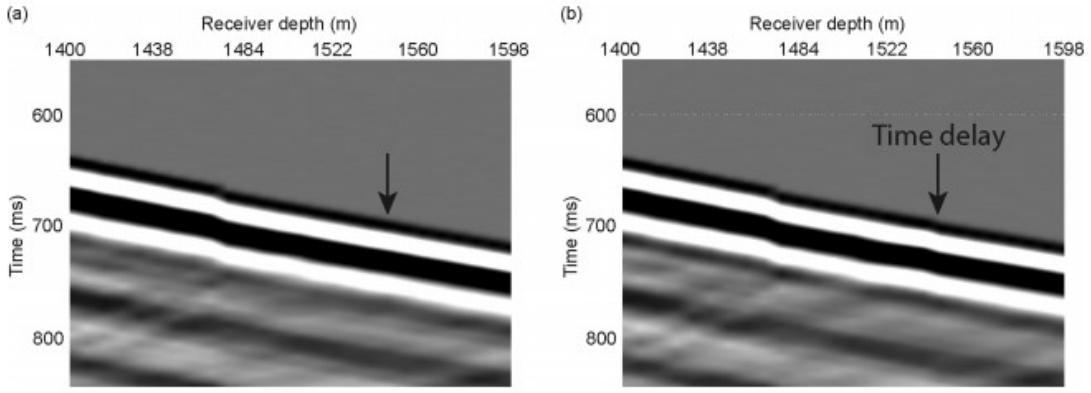

Figure 3 A zoomed section from the raw VSP shot in Fig. 2 for receiver interval 1380 m–1600 m for (a) baseline and (b) monitor. A delay in the first arrivals is indicated by the arrow in (b).

Accurately picking first-arrival times is a critical step (Dillon and Collyer 1985) since all subsequent data processing steps, wavefield separation, deconvolution, and interval velocity estimation are based on these picks. Furthermore, in a time-lapse study, our ability to estimate time delays properly relies on accurate picking of first-arrival times. Thus, it is essential to pick the time that represents the advent of the seismic energy. For dynamite sources, the wavelet is treated as the minimum phase, and the first arrivals are picked at the onset of the seismic signal (energy) as it provides the true propagation time (Chen *et al*. 2013). Such a criterion for

picking is possible for the Frio VSP data due to the high signal-to-noise ratio of the data in the vicinity of the first arrivals. We perform the picking with the data resampled to 0.1 ms. The background noise level governs our picking uncertainty for the time-lapse changes. Thus, we estimate the uncertainty in the time picks from variations between the baseline and monitor surveys above the injection interval for near-offset shots, where we do not expect any changes related to CO_2 injection. The obtained uncertainty is about ±0.2 ms.

Processing of the VSP data for P-wave reflection analysis utilizes the preprocessed data and follows a similar processing sequence as applied by Daley *et al*. (2008) where unwanted downgoing waves, shear waves, and converted waves are separated using median filtering followed by deconvolution to enhance the frequency content of the signal. We then apply normal moveout (NMO) corrections, assuming no dip using interval velocities from the baseline VSP. The signal is enhanced by applying a median filter to the NMO-corrected sections. Figure 4 shows the final processed baseline and monitor VSP sections and their difference for shot 1.

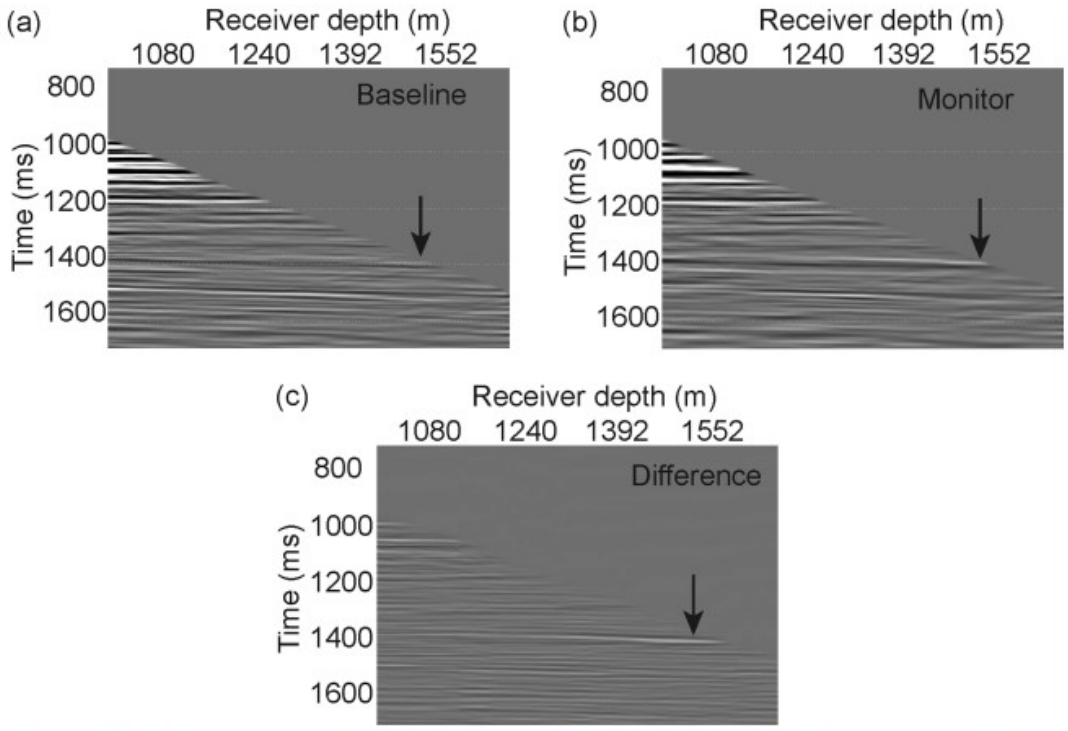

Figure 4 Processed VSP data for shot 1 using the processing flow described in the text for (a) baseline, (b) monitor, and (c) difference record. The reservoir reflection is indicated by the arrows.

VERTICAL SEISMIC PROFILE DATA ANALYSIS AND RESULTS

Transit time data

The transit time delays between the baseline and monitor VSP surveys obtained by picking the first arrivals are shown in Fig. 5(a). The time delays

are associated with a change in the velocity as supercritical CO_2 replaces brine in the pore space. A maximum time delay of 1.3 ± 0.2 ms is observed for the receiver at a depth of about 1550 m. The gamma ray log shows that this point is approximately 8.8 m below the top of the injection interval. The time delays quickly decrease for deeper receivers and vanish for the northwest and northeast offsets (not shown), suggesting that the zone of significant P-wave velocity changes has a small lateral extent in the immediate vicinity of the injection well.

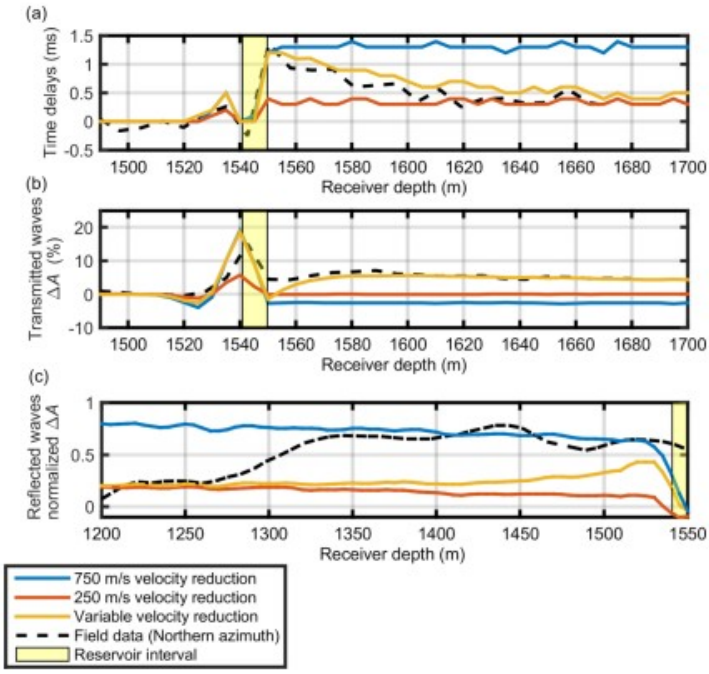

Figure 5 Time-lapse VSP for the modelling results and real data for (a) time delays, (b) first-arrival amplitude difference, and (c) reflected waves' amplitude difference. The velocity changes used in the modelling are as indicated in the legend. The layer thickness is 8.8 m, and the injection interval is shaded (yellow). The attributes shown are for an offset of 125 m. The variable velocity change based on the real data is for a CO_2 plume that extends 30 m up-dip.

We limit the analysis of time delays to near-offset shots since we are interested to investigate velocity–saturation relations (VSRs) at the vicinity of the injection well. To convert the time delays (Δt) to a change in P-wave velocity ΔV_p, we need the post-injection P-wave velocity (V_{post}). We use the initial P-wave velocity ($V_{baseline}$) and the travel distance of the ray path in the reservoir (d) to calculate the initial transit time (t_0), from which we then obtain V_{post} by:

$$V_{post} = \frac{d}{\Delta t + t_0}. \quad (1)$$

The travel distance (d) is estimated for a maximum possible plume thickness of 8.8 m, assuming a straight ray path and zero-offset geometry, which is considered adequate for receivers close to the CO_2 plume. The maximum time delay observed for the depth of about 1550 m corresponds to a velocity reduction of about 750 ± 150 m/s in the immediate vicinity of the injection well, as indicated by the peak in the shaded region in Fig. 5(a); going towards receivers below 1600 m (i.e., ray paths further away from the injection well), the velocity reduction is about 250 ± 150 m/s. The

uncertainty here is calculated using equation 1 with Δt = 0.2 ms. The obtained velocity changes will be utilized to constrain the input parameters for the rock physics model and VSR in the CO_2 VSR section.

Transmitted wave amplitudes

The direct arrival amplitude changes are related to the change in the transmission coefficient of the medium. The transmission coefficient defines the decrease in energy for the incident wave given a reflector of infinite lateral extent. However, from the travel-time results, we know that the CO_2 plume is of limited lateral extent. Additionally, the plume is expected to spread out less down-dip of the injection well than in the up-dip direction as CO_2 migrates up-dip by gravity. The plume thickness is expected to be no more than 8.8 m, which is smaller than the wavelength. Such plume geometry can result in a complex amplitude response comprising diffractions from the plume edges and interference due to tuning.

For the transmitted waves' analysis, we pick the maximum amplitudes of the first arrivals for the baseline and monitor surveys and normalize each set by its maximum amplitude. Figure 5(b) shows the amplitude difference for the normalized amplitudes of the baseline (A_b) and monitor (A_m) surveys as $(A_m - A_b) \times 100$ versus receiver depth. The amplitudes of the direct arrivals have a high signal-to-noise ratio. Variations between the time-lapse surveys above the injection interval are less than 2%, which gives us confidence that the observed changes at the top of the reservoir are caused by CO_2 injection. We obtain an amplitude increase at the reservoir top of 15 ± 2% for shot 1 and up to 18±2% for other near-offset shots (not shown). Such variations are related to the complexity of the lateral distribution of CO_2 as, at different azimuths, different CO_2 volumes near the borehole are sampled. Therefore, quantitative interpretation of these observations requires full waveform modelling.

Reflected waves analysis

Seismic waves are reflected from an area in the subsurface rather than a point. Thus, reflection amplitudes are affected by the spatial distribution of CO_2 and the magnitude of the impedance change caused by the injected CO_2 volume. To calculate the amplitude response, we investigate the root-mean-square (RMS) amplitude (A) picked over the same reservoir window for both the baseline and monitor surveys. The change in the RMS amplitude (ΔA) response of reflected waves is calculated as the normalized difference between the post-injection and pre-injection RMS amplitudes (A_{post}) and (A_{pre}), respectively, as

$$\Delta A = \frac{(A_{Post} - A_{Pre})}{\max(A_{Post} - A_{Pre})}. \quad (2)$$

The magnitude of the amplitude changes varies with azimuth, offset, and area of investigation. The maximum change in reflected wave amplitude for the near-offset shots is about ΔA = 0.8 for shot 1, as shown in Fig. 5(c). The

uncertainty of the measurement is difficult to determine as it depends on the repeatability of the whole seismic section. Figure 4(c) shows the difference record between the baseline and monitor surveys presented in Figs. 4(a) and 4(b). The normalized RMS repeatability metrics (Kragh and Christie 2002) in this difference record ranges between 20% and 160% (not shown). Thus, fluctuations in the recorded reflection amplitudes are attributed to both noise and the effect of the CO_2 plume. Similar to the transmitted wave amplitudes, the reflection amplitude changes are difficult to interpret without the support of synthetic modelling that can take into account the finite lateral extent of the plume. Thus, in the next section, we perform 2.5D elastic, finite-difference modelling.

Finite-difference modelling

The seismic response is controlled by many factors such as the acoustic impedance and the lateral extent and thickness of the reservoir. Thus, to understand the time-lapse seismic response of both travel-time and amplitude changes, we perform a 2.5D elastic, finite-difference modelling study that refers to a 3D wave propagation over a 2D model of the subsurface (Costa, Neto, and Novais 2006; Kostyukevych *et al*. 2008). This will aid the quantitative interpretation of the field measurements and later in the VSR.

To this end, we create a 2D elastic model using P-wave velocity, S-wave velocity, and density from existing baseline well logs for the reservoir interval where available (Fig. 6) and VSP interval velocities for the shallow part to the surface. Three post-injection models with various velocity and density changes are considered. The first model assumes a velocity reduction of 750 m/s over the reservoir interval, which is similar in magnitude to the velocity reduction estimated from the field data. The second model assumes a 250-m/s velocity reduction in the same reservoir interval. In both models, the plume is represented as a flat continuous layer (no plume edges or tapering of the velocity). For the third model, we introduce a laterally variable velocity (keeping the reservoir thickness constant) by interpolating from the 750 m/s V_p reduction at the injection well to the baseline model velocity 30 m away from the injection well. In all models, we assume horizontal layering for simplicity. This assumption is adequate for near-offset shots and a limited plume extent. The extent of the 2D elastic model is 2 km x 3 km with a grid spacing of 1 m x 1 m. A 50-Hz zero-phase Ricker wavelet is used as a source.

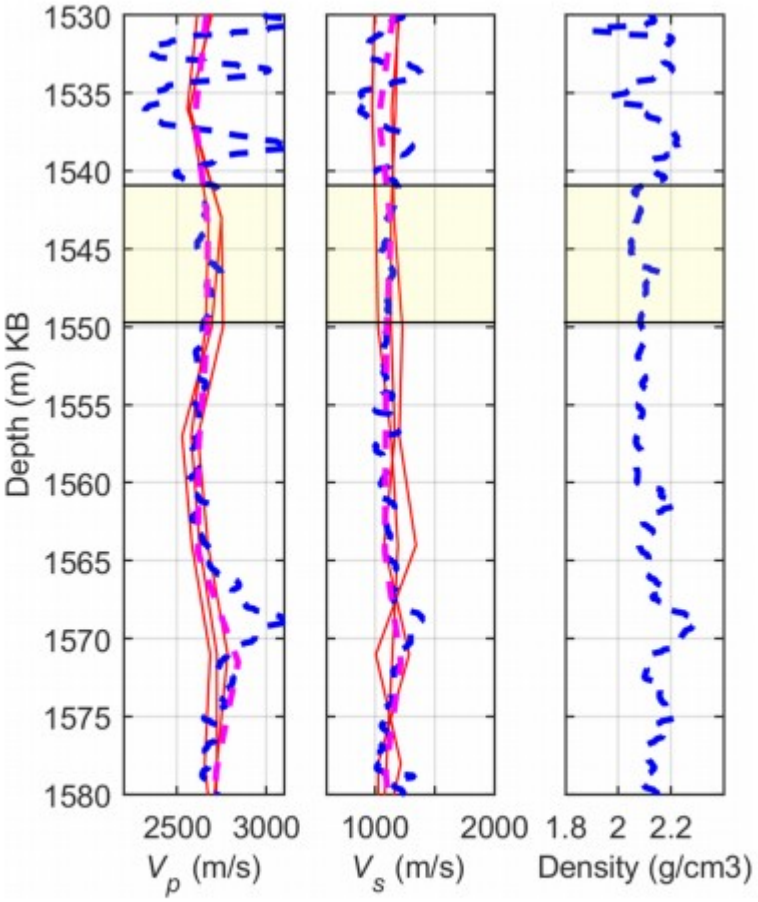

Figure 6 Baseline V_p, V_s, and density logs for the injection well. The Frio "C" interval of interest is shaded. Interval velocities from VSP shown for near-offset shots (red lines). The upscaled well log velocities (dashed magenta) show good agreement for both V_p and V_s.

The synthetic data were processed with a similar processing sequence as the field data. However, since we are using a zero-phase Ricker wavelet, we pick the time of the peak amplitude to obtain the first arrivals. Both the variable and constant velocity models give a similar peak value in the travel-time delays of 1.2 ± 0.1 ms near the injection well, which is comparable with the maximum travel-time delay obtained from the field data. However, as we go towards deeper receivers, the variable velocity model best matches with the field data [see Fig. 5(a)]. The first-arrival amplitudes show a peak amplitude change of 19 ± 2 % for both models that is of the same order as for the field data. Again, the lateral variable model fits the field data better for deeper receivers [see Fig. 5(b)]. The reflection RMS amplitudes show a peak response of 0.1, 0.8, and 0.43 for the 250 m/s, 750 m/s, and variable velocity models respectively [see Fig. 5(c)]. We note that, for the variable velocity model, the recorded reflection amplitude response decreases for shallower receivers. This effect is also observed in field data. These effects are caused

by a limited plume extent. We attribute the mismatch between the field reflection amplitude and the modelling to the complex geometry of the plume and noise levels in the field reflection data. Moreover, as the plume spread is small, the reflection response rapidly decays for shallower receivers as the Fresnel zone becomes larger. It is shown in Figs. 5(a), 5(b), and 5(c) that a 750-m/s velocity change best matches the peak time-lapse changes of the field data (i.e., travel-time delays, transmitted wave amplitudes, and reflected wave amplitudes) for receivers in the proximity of the reservoir.

ROCK PHYSICS MODELLING OF VELOCITY CHANGES

To interpret the observed time-lapse seismic changes in terms of fluids saturation, a rock physics model linking velocity and saturation is required.

Rock physics model

The choice of a theoretical or empirical equation to derive the frame properties of rocks depends on the type of the rock and the available data. The injection unit in the Frio “C” formation is a relatively homogenous sandstone with high porosity; thus, an attractive option is to use Gassmann's equation (Gassmann 1951) to model it. However, one must obtain all the input parameters for the model preferably from field measurements. Assumptions and validity of Gassmann's fluid substitution have been widely discussed in the literature (e.g., Berryman 1999; Nolen-Hoeksema 2000; Smith *et al*. 2003; Han and Batzle 2004; Grochau and Gurevich 2009). Gassmann's equation can be written as

$$K_{sat} = K_{dry} + \frac{\left(1 - \frac{K_{dry}}{K_g}\right)^2}{\frac{\phi}{K_{fl}} + \frac{1-\phi}{K_g} - \frac{K_{dry}}{K_g^2}}, \quad (3)$$

where K_{sat}, K_{dry}, K_{fl}, K_g, and ϕ are the bulk modulus of the saturated rock, the bulk modulus of the dry frame, the bulk modulus of the fluids, the bulk modulus of the grains, and the porosity, respectively.

Input parameters for Gassmann's equation (Gassmann 1951) can be obtained from laboratory measurements or field data such as well logs. Quality control of these input parameters is essential to reduce the uncertainty in applying the fluid replacement equation. In the following, we provide a description of how we obtain these input parameters from the available data.

Grain properties

The mineralogical composition of the Frio “C” sandstone is not well constrained, but quartz, orthoclase, and plagioclase feldspar and rock fragments have been reported from core analysis and X-ray diffraction (Hovorka *et al*. 2006; Sakurai *et al*. 2006). Thus, we initially assumed a constant feldspar content of 20% typical of that reported in literature,

whereas a variable clay and quartz content is used based on the gamma ray log (see Fig. 7).

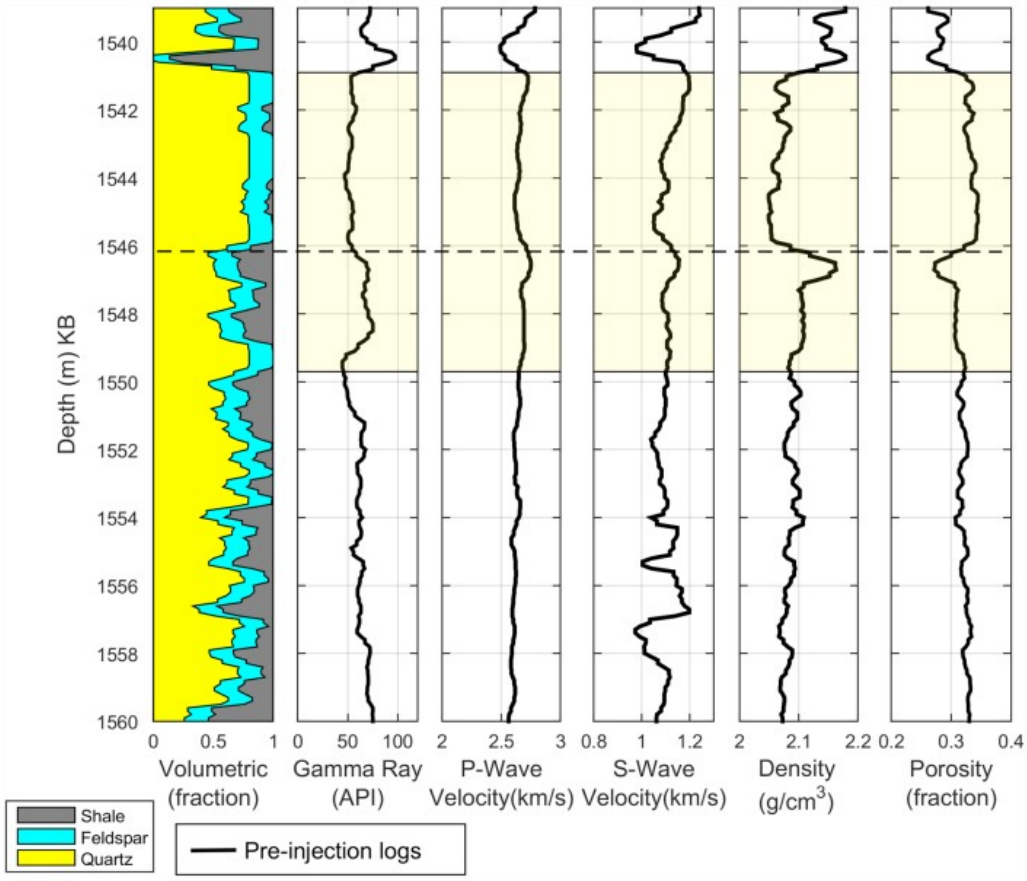

Figure 7 Frio formation mineralogical composition from GR log and literature, V_p, V_s, density, and porosity logs. The reservoir interval used in the modelling is shaded. Dashed line indicates the boundary between the upper clean sandstone and lower shaley sandstone.

The effective modulus for the mixture of solid constituents is determined using the arithmetic average of the Hashin–Shtrikman bounds (Hashin and Shtrikman 1963). This average does not take into account the complex geometrical factors involved in grain mixtures, but it provides a reasonable first-order approximation especially when the lower and upper bounds are not too far apart. Unfortunately, with the limited information about the mineral constituents, the obtained bulk and shear moduli can strongly vary, as shown in Table 1. Thus, the effect of the grain modulus on the VSR is investigated closely later in the VSR section.

Table 1 Density and moduli of minerals used in the initial Frio "C" rock physics modelling (Mavko *et al.* 2009).

constituent	Density (kg/m^3)	K (GPa)	μ (GPa)
Quartz	2650	37.0	45.0
Feldspar (Plagioclase)	2630	75.6	25.0
Clay (Highly variable)	2260	25.0	9.0

Fluid properties and saturations

The fluid properties of the *in situ* brine and injected CO_2 at reservoir conditions of 55°C and effective pressure of 15 MPa are shown in Table 2 (Batzle and Wang 1992). CO_2 at these reservoir conditions is in a supercritical state.

Table 2 Brine and CO_2 properties at reservoir conditions. * Supercritical CO_2 (Daley *et al.* 2008; The National Institute of Standards and Technology 2014)

	K (GPa)	Density (kg/m^3)
Brine	2.75	1030
CO_2*	0.07	653

The fluid mixture of two immiscible fluids could be uniform or patchy (Masson and Pride 2011). Hence, the choice of a mixing law for the fluids determines the magnitude of the P-wave velocity change predicted by the fluid replacement scheme. Assuming a uniform homogenous mixture of fluid phases, Wood's equation (Mavko, Mukerji, and Dvorkin 2009) can be used to calculate the effective bulk modulus of the fluids (K_{fl})

$$K_{fl} = \left[\frac{S_{brine}}{K_{brine}} + \frac{S_{CO_2}}{K_{CO_2}} \right]^{-1}, \quad (4)$$

where K_{brine} is the bulk moduli of brine, S_{brine} is the saturation of brine, K_{CO_2} is the bulk moduli of CO_2, and S_{CO_2} is the saturation of CO_2. This mixing law predicts the maximum velocity reduction for any given mixture of brine and CO_2. If we assume a patchy saturation case, then, for a given mixture of CO_2 and brine, the absolute P-wave velocity change will be less than or equal to that predicted by Wood's equation. However, given that the observed velocity changes in the time-lapse VSP data are large, we use Wood's equation to model for the maximum velocity change due to CO_2 saturation. The density of the CO_2 and brine fluid mixture is given by

$$\rho_{fl} = \rho_{brine} S_{brine} + (1 - S_{brine}) \rho_{CO_2}. \quad (5)$$

where ρ_{brine} and ρ_{CO_2} are the brine and CO_2 densities at reservoir conditions, respectively.

Fluids saturation is a common unknown in many time-lapse studies. In the Frio project, CO_2 saturation was inferred using the Schlumberger reservoir saturation tool (Hovorka *et al*. 2006; Sakurai *et al*. 2006; Doughty *et al*. 2008). However, there was no reliable saturation estimation for some parts of the injection reservoir interval after the monitor seismic survey due to wellbore issues related to the casing deployment (Hovorka *et al*. 2006). Thus, we consider CO_2 saturation in the range of 0.18–0.62 after injection at the injection well based on the available data (Hovorka *et al*. 2006; Sakurai *et al*. 2006).

Porosity

Another parameter needed in order to use Gassmann's equation is the porosity of the rock frame. An average porosity of 32% was obtained from core measurements for the injection interval (see Fig. 8) (Sakurai *et al*. 2006). The porosity in the upper 5 m of the formation interval is around 34%, whereas for the lower shaley interval, the porosity decreases to about 28%. We use these core values to calibrate our porosity log calculated from density, as shown in Fig. 7. An overall good agreement for the injection interval is obtained.

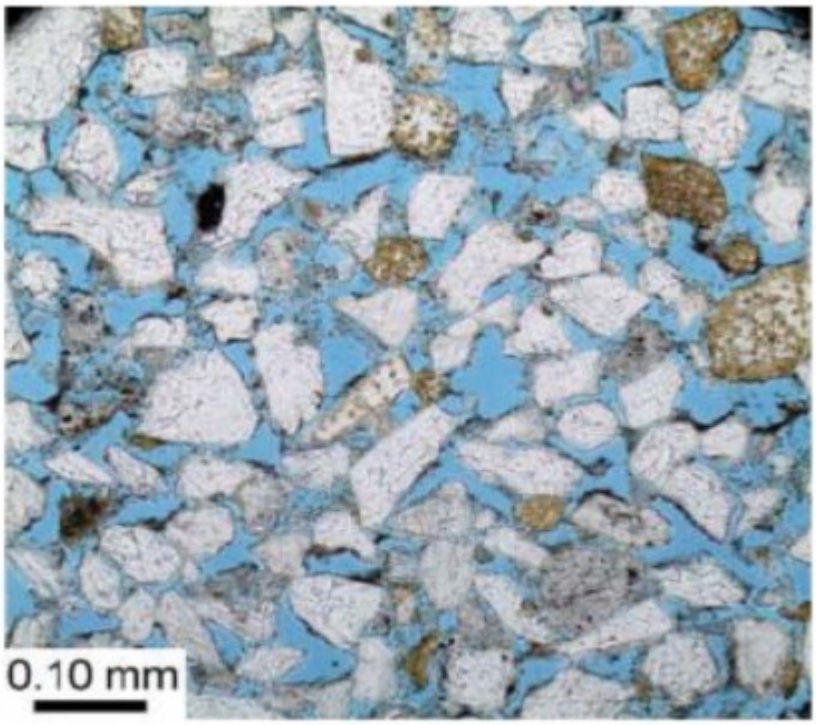

Figure 8 Thin section of the high-porosity and high-permeability Frio "C" sandstone. Pore space appears in blue (Sakurai *et al.* 2006).

Drained frame properties

The dry-frame bulk modulus is the most important variable in the fluid substitution scheme. Often the dry-frame bulk modulus K_{dry} from laboratory measurements is unknown and the drained frame bulk modulus ($K_{drained}$) is obtained by rewriting Gassmann's equation, assuming the knowledge of K_{sat} (Zhu and McMechan 1990; Engelmark 2002; Smith *et al*. 2003).

A common approach in the oil and gas industry is to utilize wireline measurements of the brine-saturated intervals of the reservoir of interest to obtain K_{sat} (Engelmark 2002). However, this approach requires careful checking of the input parameters: P-wave velocity (V_p), S-wave velocity (V_s), and the density of the saturated rock frame (ρ_b). Inputting wrong values can result in large errors or even unphysical values of $K_{drained}$ (Kazemeini, Juhlin, and Fomel 2010). To examine the baseline sonic measurements, we employ the interval velocities obtained from the VSP data. As the VSP interval velocities are at a different scale compared with the sonic logs, upscaling of the log velocities is performed using Backus averaging (Mavko *et al*. 2009). The upscaled log velocities and VSP interval velocities show good agreement (see Fig. 6).

After insuring the quality of the input log velocities, we first calculate the bulk (K_{sat}) and shear moduli (μ_{sat}) of the *in situ* brine-saturated rock from the baseline V_p, V_s, and ρ_b logs:

$$K_{sat} = \rho_b \left(V_p^2 - \frac{4}{3} V_s^2 \right). \quad (6)$$

$$\mu_{sat} = \rho_b V_S^2. \quad (7)$$

Second, the drained frame bulk ($K_{drained}$) and shear moduli ($\mu_{drained}$) are calculated using inverse Gassmann's equations (Zhu and McMechan 1990)

$$K_{drained} = \frac{K_{sat}\left(\frac{\phi K_g}{K_{fl}} + 1 - \phi\right) - K_g}{\frac{\phi K_g}{K_{fl}} + \frac{K_{sat}}{K_g} - 1 - \phi}. \quad (8)$$

$$\mu_{drained} = \mu_{sat}. \quad (9)$$

The density of the drained frame ($\rho_{drained}$) is calculated with the following equation:

$$\rho_{drained} = \rho_b - \rho_{brine}\phi. \quad (10)$$

The calculated drained frame bulk and shear moduli are held constant during subsequent fluids substitution. Such an assumption may be invalid if the drained frame properties change during fluid replacement, e.g., as the case with formation damage by pressure or chemical interaction of the fluids with the frame-forming minerals. If a change is observed in the bulk and shear moduli of the drained frame, then its properties should be updated.

Constraining CO_2 velocity–saturation relation

The bulk moduli of a saturated rock can be calculated given the fluid and frame properties. We perform the Gassmann fluid substitution (Gassmann 1951) using equation 3 with the calculated parameters from the previous steps with Gassmann–Wood, which predicts the maximum fluid effect on the saturated rock frame. The uncertainty of the drained frame properties and subsequent VSR are difficult to quantify. However, given the good constraints on the input parameters, we expect the model to present the Frio “C” formation adequately.

The initial values for the input parameters for the VSR are listed in Table 3. We consider for the post-injection CO_2 saturation values in the range of 0.18–0.62 (Hovorka *et al*. 2006; Sakurai *et al*. 2006). The resulting nominal VSR for uniform saturation is shown by a blue line in Fig. 9(a) along with the velocity change estimated from time-lapse VSP (vertical black line). Note that the velocity reduction predicted by the Gassmann fluid substitution for any CO_2 saturation is less than that observed in the time-lapse VSP. This is true even when taking into account the uncertainty in the time picks for the first-arrival travel-time delays. The same observation can be made from the transmission coefficients: the change in the transmission coefficient (ΔI_p) calculated from the rock physics model is much lower than that obtained

from time-lapse VSP [see Fig. 9(b)], indicating that we cannot predict such a large ΔI_p. We recall here the reflection amplitude analysis and the modelling results, which also showed that our field observations at the injection well are consistent with about 750 m/s reduction in V_p [see Fig. 5(c)]. These observations are from three independent attributes, and all of them suggest that the rock physics model underestimates the velocity change occurring around the injection well.

Table 3 Nominal model properties for the Frio "C" sandstone used as input for calculating the saturated frame properties and subsequent VSR calculations

V_p (m/s)	V_s (m/s)	Density (Kg/m^3)	K_{fl} (GPa)	Porosity	K_g (GPa)
2648	1117	2075	2.75	0.33	42.2

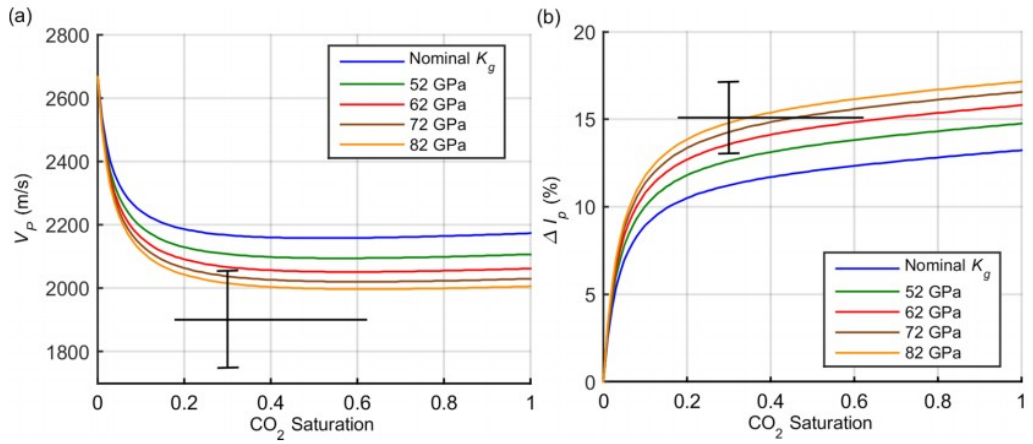

Figure 9 The VSR for the Frio "C" sandstone with changing grain bulk moduli. (a) The peak velocity reduction estimated from the time-lapse VSP shown in Fig. 5 (a) with the uncertainty (vertical bar). (b) The transmission coefficient change as a function of CO_2 saturation, the vertical bar is that obtained from the real VSP first arrivals peak amplitude change in Fig. 5 (b). The control on CO_2 saturation (horizontal bar) is from the saturation logs range at the injection well from Doughty *et al.* (2008).

To investigate this discrepancy, we look at the largest uncertainty in the rock physics model for the Frio "C" interval, which are the grain properties. A way to evaluate the sensitivity of our model to K_g is by perturbing the input values of K_g for the calculation of the drained frame properties (inverse Gassmann). We keep the model parameters in Table 3 constant except for K_g, which is changed from the initial value by an increment of 10 GPa up to 82 GPa. The VSRs with changing K_g are shown in Fig. 9(a); we see that we need a K_g over 70 GPa to match the observations. Similarly, to explain the transmission coefficient change observed in the field, a K_g value of more than

52 GPa is required [see Fig. 9(b)]. Such large values of the grain modulus are inconsistent with the predominant quartz mineralogy of the formation.

DISCUSSION

We have shown that neither the large time-lapse VSP anomalies for first arrivals nor reflection amplitudes could be explained by the Gassmann fluid substitution even when taking uncertainty in field measurements into account. Time-lapse VSP has provided three independent attributes, namely, direct arrival travel times, first-arrival amplitudes, and reflection amplitudes. The most robust quantitative measure here is the travel-time delay, which has a smaller uncertainty in comparison with the amplitudes. For the direct arrivals, we observe a maximum time delay of about 1.3 ± 0.2 ms that corresponds to a P-wave velocity reduction of about 750 ± 150 m/s. The constrained rock physics model for the Frio “C” reservoir does not predict such large reduction in V_p.

What could be the reason for this discrepancy? Since the effect of injected CO_2 on elastic properties was estimated using Gassmann's equation, it might be possible that one or more of the assumptions of Gassmann's theory are violated. To this end, we assess the applicability of the main assumptions of Gassmann's theory in the context of this case study:

The rock frame is isotropic on both microscale and macroscale (Brown and Korringa 1975). Since nearly all minerals are anisotropic, the assumption of isotropy on the microscale is never satisfied exactly. However, an assumption is usually made that anisotropic mineral grains with random (isotropic) distribution of orientations mixed on a fine scale result in a medium nearly isotropic on the grain scale. Furthermore, sandstones are commonly assumed to be relatively isotropic on a macroscale. This suggests that the effect of any anisotropy on the fluid substitution is likely to be small.

The rock frame is homogeneous on the microscale, i.e., it is made of a single mineral (Mavko *et al*. 2009). Since the Frio “C” sandstone consists mainly of quartz, this assumption is approximately valid, and any micro-heterogeneity is unlikely to cause significant deviations from the predictions of Gassmann's theory.

Both the rock frame and the fluid are also homogeneous on the macroscale (Mavko *et al*. 2009), which is on a scale of a representative volume. The injection interval in Frio “C” is fairly homogeneous, but the fluid distribution might not be uniform. Yet, any deviation from uniform distribution would result in even higher saturated bulk modulus and, hence, even larger discrepancy than for uniform saturation and therefore cannot explain our discrepancy.

The fluid pressure is uniform throughout the pore space in a representative volume of the rock (relaxed regime). This assumption is satisfied when the pore pressure has sufficient time to equilibrate within one half-cycle of the wave, i.e., when the wave frequency is much lower than the squirt frequency

(Mavko *et al*. 2009). This assumption is always assumed to be satisfied at seismic frequencies, at least for the high-porosity and high-permeability rocks such as Frio “C” sandstone.

Finally, Gassmann's theory assumes that the rock frame properties do not change with the change of the pore fluid (Mavko *et al*. 2009). This appears to be the only assumption that can be violated and could explain the large *Vp* reduction observed. That is, it is possible that injection of CO_2 into the pore space could have caused some physical or geochemical processes that can result in the weakening of the rock frame.

Previous studies of crosswell travel-time tomography at the Frio site have reported that the large P-wave reduction at the injection well is accompanied by a reduction in S-wave velocities of more than 220 m/s (Daley *et al*. 2008). Such a large change in S-wave velocity is not predicted by the Gassmann fluid substitution as the shear moduli is constant according to equation 9. Moreover, according to the same equation, any density change by injecting a lower density fluid (CO_2 in this case) would cause an S-wave velocity increase rather than a decrease. Rock frame changes during fluid injection could be caused by many factors, including pressure effects by fluid injection (Saul and Lumley 2015) or, in the case of injecting reactive fluid such as CO_2, by geochemical interactions that alter the rock-frame-forming mineral (Marbler *et al*. 2013).

We first investigated pressure changes associated with CO_2 injection as a possible cause of frame weakening. However, in the Frio project, the maximum effective pressure decrease was less than 0.5 MPa (Sakurai *et al*. 2006); such a small pressure decrease is not expected to cause significant velocity changes for an initial reservoir effective pressure above 15 MPa (Makse *et al*. 1999). Indeed, according to Eberhart-Phillips, Han, and Zoback (1989), at such reservoir conditions, P-wave and S-wave velocity changes due to such pore pressure increase are less than 30 m/s, which is much smaller than the magnitude of the velocity changes observed in the time-lapse VSP data.

On the other hand, geochemical analysis has suggested that CO_2 caused the dissolution of rock-forming minerals (Kharaka *et al*. 2006). Rock frame changes, if induced by geochemical processes, are difficult to quantify without independent measurement. The frame shear modulus is not affected by saturation changes (according to the Gassmann fluid substitution) and thus could provide information of changes in the rock frame. Hence, S-waves could be a possible source of such information. Unfortunately, we were unable to obtain the time-lapse changes for the S-wave interval velocities from the VSP data due to the insufficient signal-to-noise ratio for S-wave arrivals.

Our rock physics model based on the Gassmann fluid substitution (Gassmann 1951) can only handle mechanical changes caused by the pore fluid interacting with the rock frame. Thus, we suggest that an alternative model

is required to handle possible non-elastic factors in the reservoir drained frame properties after fluid injection. Such a model should allow the variation of the drained frame shear and bulk moduli based on field observations. This will be investigated in a separate paper.

CONCLUSIONS

Verifying the applicability of theoretical rock physics models to interpret field data is crucial for quantitative time-lapse seismic analysis. In this paper, we have investigated the use of Gassmann's equation to constrain the velocity–saturation relationship for high-porosity sandstone using time-lapse VSP data of the Frio CO_2 injection project. The time-lapse VSP data have shown large travel-time delays for the post-injection survey. We estimated this travel-time delay to be caused by a velocity reduction of 750 ± 150 m/s at the injection well. Observed first-arrival amplitude changes and reflection amplitudes, as well as the 2.5D elastic, finite-difference modelling results, support the estimates of the magnitude of this velocity change. We created a site-specific rock physics model from existing field measurement using Gassmann's equation for a uniform saturation case. It became apparent that our rock physics model underestimates the velocity change obtained from the field observations at the injection well. This discrepancy suggests the presence of formation damage, which weakened the rock frame after CO_2 injection. Our study highlights the need of verifying the applicability of theoretical rock physics models to describe fluid–rock physics relationships. Moreover, an alternative model is required, which incorporates non-elastic changes in the rock frame caused by CO_2 injection to explain the measured data. Understanding these effects on the rock physics relationship is important for the accurate use of time-lapse seismic data to estimate CO_2 saturation in the subsurface.

ACKNOWLEDGEMENTS

This work has been funded by the Commonwealth of Australia through its Cooperative Research Centre Program to support Cooperative Research Centre for Greenhouse Gas Technologies research and by the sponsors of the Curtin Reservoir Geophysics Consortium. The authors would like to thank Lawrence Berkeley National Laboratory (LBNL) for providing the data for this study. Work at LBNL was supported by the Office of Fossil Energy, U.S. Department of Energy, under Contract DE-AC0205CH11231.

REFERENCES

Arts R., Eiken O., Chadwick A., Zweigel P., van der Meer L. and Zinszner B. 2004. Monitoring of CO_2 injected at Sleipner using time-lapse seismic data. *Energy* 29, 1383– 1392.

Batzle M. and Wang Z.J. 1992. Seismic properties of pore fluids. *Geophysics* 57, 1396– 1408.

Berryman J.G. 1999. Origin of Gassmann's equations. *Geophysics* 64, 1627–1629.

Brown R.J. and Korringa J. 1975. On the dependence of the elastic properties of a porous rock on the compressibility of the pore fluid. *Geophysics* 40, 608–616.

Carcione J.M., Picotti S., Gei D. and Rossi G. 2006. Physics and seismic modeling for monitoring CO_2 storage. *Pure and Applied Geophysics* 163, 175–207.

Chadwick A., Williams G., Delepine N., Clochard V., Labat K., Sturton S. *et al*. 2010. Quantitative analysis of time-lapse seismic monitoring data at the Sleipner storage operation. *The Leading Edge* 29, 170– 177.

Chen Y., Li Y., Zhao H., Gao X. and Qiu Y. 2013. Study of first arrival time of VSP data. In: *Near Surface Geophysics Asia Pacific Conference, Beijing, China, 17–19 July 2013*, pp. 97–101.

Costa J., Neto F.S. and Novais A. 2006. 2.5 D Elastic finite-difference modeling. 68th EAGE Conference and Exhibition.

Daley T.M., Myer L., Peterson J.E., Majer E.L. and Hoversten G.M. 2008. Time-lapse crosswell seismic and VSP monitoring of injected CO_2 in a brine aquifer. *Environmental Geology* 54, 1657– 1665.

Dillon P. and Collyer V. 1985. On timing the VSP first arrival. *Geophysical Prospecting* 33, 1174– 1194.

Doughty C., Freifeld B.M. and Trautz R.C. 2008. Site characterization for CO_2 geologic storage and vice versa: The Frio brine pilot, Texas, USA as a case study. *Environmental Geology* 54, 1635– 1656.

Eberhart-Phillips D., Han D.-H. and Zoback M.D. 1989. Empirical relationships among seismic velocity, effective pressure, porosity, and clay content in sandstone. *Geophysics* 54, 82– 89.

Engelmark F. 2002. Error propagation in Gassmann modeling for 4D feasibility studies. *The Leading Edge* 21, 984– 987.

Gassmann F. 1951. Elastic waves through a packing of spheres. *Geophysics* 16, 673– 685.

Grochau M. and Gurevich B. 2009. Testing Gassmann fluid substitution: Sonic logs versus ultrasonic core measurements. *Geophysical Prospecting* 57, 75–79.

Han D.-h. and Batzle M.L. 2004. Gassmann's equation and fluid-saturation effects on seismic velocities. *Geophysics* 69, 398– 405.

Hardage B.A. 1985. *Vertical Seismic Profiling*. Pergamon Press.

Hashin Z. and Shtrikman S. 1963. A variational approach to the theory of the elastic behaviour of multiphase materials. *Journal of the Mechanics and Physics of Solids* 11, 127– 140.

Hovorka S. 2009. Frio brine pilot: The first US sequestration test. *Southwest Hydrology* 8, 26– 31.

Hovorka S.D., Benson S.M., Doughty C., Freifeld B.M., Sakurai S., Daley T.M. *et al*. 2006. Measuring permanence of CO_2 storage in saline formations: The Frio experiment. *Environmental Geosciences* 13, 105– 121.

Ivandic M., Yang C., Lüth S., Cosma C. and Juhlin C. 2012. Time-lapse analysis of sparse 3D seismic data from the CO_2 storage pilot site at Ketzin, Germany. *Journal of Applied Geophysics* 84, 14– 28.

Ivanova A., Kashubin A., Juhojuntti N., Kummerow J., Henninges J., Juhlin C. *et al*. 2012. Monitoring and volumetric estimation of injected CO_2 using 4D seismic, petrophysical data, core measurements, and well logging: A case study at Ketzin, Germany. *Geophysical Prospecting* 60, 957– 973.

Johansen T., Jensen E., Mavko G. and Dvorkin J. 2013. Inverse rock physics modeling for reservoir quality prediction. *Geophysics* 78, M1– M18.

Kazemeini S.H., Juhlin C. and Fomel S. 2010. Monitoring CO_2 response on surface seismic data; a rock physics and seismic modeling feasibility study at the CO_2 sequestration site, Ketzin, Germany. *Journal of Applied Geophysics* 71, 109– 124.

Kharaka Y., Cole D., Hovorka S., Gunter W., Knauss K. and Freifeld B. 2006. Gas-water-rock interactions in Frio Formation following CO_2 injection: Implications for the storage of greenhouse gases in sedimentary basins. *Geology* 34, 577– 580.

Kharaka Y.K., Thordsen J.J., Hovorka S.D., Seay Nance H., Cole D.R., Phelps T.J. *et al*. 2009. Potential environmental issues of CO_2 storage in deep saline aquifers: Geochemical results from the Frio-I Brine Pilot test, Texas, USA. *Applied Geochemistry* 24, 1106– 1112.

Kostyukevych A., Marmalevskyi N., Roganov Y. and Tulchinsky V. 2008. Anisotropic 2.5 D-3C finite-difference modeling. 70th EAGE Conference and Exhibition.

Kragh E. and Christie P. 2002. Seismic repeatability, normalized rms, and predictability. *The Leading Edge* 21, 640– 647.

Lumley D., Adams D., Wright R., Markus D. and Cole S. 2008. Seismic monitoring of CO_2 geosequestration: Realistic capabilities and limitations. In: *SEG Technical Program Expanded Abstracts*, pp. 2841–2845.

Lumley D.E. 2001. Time-lapse seismic reservoir monitoring. *Geophysics* 66, 50– 53.

Lüth S., Bergmann P., Cosma C., Enescu N., Giese R., Götz J. *et al*. 2011. Time-lapse seismic surface and down-hole measurements for monitoring CO_2 storage in the CO_2SINK project (Ketzin, Germany). *Energy Procedia* 4, 3435–3442.

Makse H.A., Gland N., Johnson D.L. and Schwartz L.M. 1999. Why effective medium theory fails in granular materials. *Physical Review Letters* 83, 5070.

Marbler H., Erickson K.P., Schmidt M., Lempp C. and Pöllmann H. 2013. Geomechanical and geochemical effects on sandstones caused by the reaction with supercritical CO_2: An experimental approach to in situ conditions in deep geological reservoirs. *Environmental Earth Sciences* 69, 1981– 1998.

Masson Y. and Pride S. 2011. Seismic attenuation due to patchy saturation. *Journal of Geophysical Research: Solid Earth (1978–2012)* 116.

Mavko G., Mukerji T. and Dvorkin J. 2009. *The Rock Physics Handbook: Tools for Seismic Analysis of Porous Media*. Cambridge University Press.

Michael K., Golab A., Shulakova V., Ennis-King J., Allinson G., Sharma S. *et al*. 2010. Geological storage of CO_2 in saline aquifers—A review of the experience from existing storage operations. *International Journal of Greenhouse Gas Control* 4, 659– 667.

Nolen-Hoeksema R.C. 2000. Modulus-porosity relations, Gassmann's equations, and the low-frequency elastic-wave response to fluids. *Geophysics* 65, 1355– 1363.

O'Brien J., Kilbride F. and Lim F. 2004. Time-lapse VSP reservoir monitoring. *The Leading Edge* 23, 1178– 1184.

Sakurai S., Ramakrishnan T., Boyd A., Mueller N. and Hovorka S. 2006. Monitoring saturation changes for CO_2 sequestration: Petrophysical support of the Frio brine pilot experiment. *Petrophysics* 47, 483– 496.

Saul M. and Lumley D. 2015. The combined effects of pressure and cementation on 4D seismic data. *Geophysics* 80, WA135– WA148.

Smith T., Sondergeld C. and Rai C. 2003. Gassmann fluid substitutions: A tutorial. *Geophysics* 68, 430– 440.

The National Institute of Standards and Technology. 2014. Thermophysical Properties of Carbon dioxide. http://webbook.nist.gov/cgi/fluid.cgi?ID=C124389 and Action=Page. Cited Dec 17, 2014.

Yang D., Malcolm A., Fehler M. and Huang L. 2014. Time-lapse walkaway vertical seismic profile monitoring for CO_2 injection at the SACROC enhanced oil recovery field: A case study. *Geophysics* 79, B51– B61.

Zhou R., Huang L., Rutledge J.T., Fehler M., Daley T.M. and Majer E.L. 2010. Coda-wave interferometry analysis of time-lapse VSP data for monitoring

geological carbon sequestration. *International Journal of Greenhouse Gas Control* 4, 679– 686.

Zhu X. and McMechan G.A. 1990. Direct estimation of the bulk modulus of the frame in a fluid-saturated elastic medium by Biot theory. 60th SEG annual international meeting, SEG Expanded Abstracts, vol. 9, p. 787.